

# Phase-Aware Mixture of Experts for Agentic Reinforcement Learning

Shengtian Yang<sup>1,3</sup>, Yu Li<sup>1</sup>, Shuo He<sup>2</sup>, Yewen Li<sup>3</sup>, Qingpeng Cai<sup>3</sup>, Peng Jiang<sup>3</sup>, Lei Feng<sup>1\*</sup>,

<sup>1</sup>School of Computer Science and Engineering, Southeast University, Nanjing, China

<sup>2</sup>Nanyang Technological University

<sup>3</sup>Kuaishou Technology

yangshengtian@kuaishou.com, fenglei@seu.edu.cn

## Abstract

Reinforcement learning (RL) has equipped LLM agents with a strong ability to solve complex tasks. However, existing RL methods normally use a *single* policy network, causing *simplicity bias* where simple tasks occupy most parameters and dominate gradient updates, leaving insufficient capacity for complex tasks. A plausible remedy could be employing the Mixture-of-Experts (MoE) architecture in the policy network, as MoE allows different parameters (experts) to specialize in different tasks, preventing simple tasks from dominating all parameters. However, a key limitation of traditional MoE is its token-level routing, where the router assigns each token to specialized experts, which fragments phase-consistent patterns into scattered expert assignments and thus undermines expert specialization. In this paper, we propose **Phase-Aware Mixture of Experts (PA-MoE)**. It first features a lightweight *phase router* that learns latent phase boundaries directly from the RL objective without pre-defining phase categories. Then, the phase router allocates temporally consistent assignments to the same expert, allowing experts to preserve phase-specific expertise. Experimental results demonstrate the effectiveness of our proposed PA-MoE. Code is available at <https://anonymous.4open.science/r/PA-MoE-576C/>.

## Introduction

Reinforcement learning (RL) has equipped LLM agents with a strong ability to solve complex tasks such as embodied navigation (Shridhar et al. 2021) and web interaction (Yao et al. 2022). However, most RL-based agents use a single policy network throughout an episode, causing *simplicity bias*, as shown in Figure 1(a): since simple tasks are more frequent and easier to optimize, they dominate gradient updates and occupy most of the network’s representational capacity, leaving insufficient capacity for complex tasks. For example, existing methods suffer from this limitation. RLOO (Ahmadian et al. 2024) optimizes a single policy network and reduces variance through leave-one-out baselines, but its shared parameters are still biased toward high-frequency simple patterns. GRPO (Shao et al. 2024) uses group-relative rewards to form advantages without a critic; however, when simple and complex tasks are mixed in the same batch, the larger gradients from easily-solved simple tasks overshadow the learning signal from complex ones. GiGPO (Feng et al. 2025) refines

\*Corresponding author.

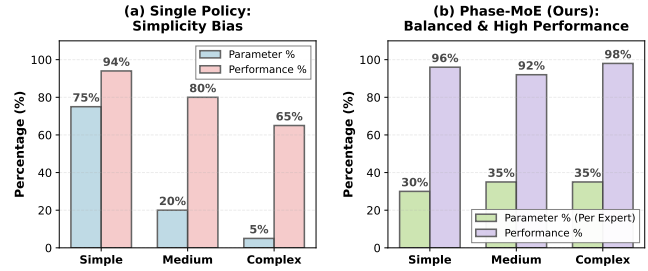


Figure 1: **Single-Policy Networks vs. Our PA-MoE.** (a) Single-policy networks exhibit severe simplicity bias: simple tasks (pick\_and\_place) occupy 75% of parameters while complex tasks (heat/cool/clean requiring multi-step tool interaction) receive only 5%. Parameter occupancy is measured as the fraction of training batches where each task category contributes  $>50\%$  of the batch loss. (b) PA-MoE achieves balanced parameter allocation ( $\sim 30\%$  per expert) and uniformly high performance across all task difficulties (96%-92%-98%).

learning signals with hierarchical group-relative advantages for multi-step trajectories, yet the underlying single-policy architecture still conflates task difficulties, causing simple sub-tasks to dominate parameter updates.

Fortunately, Mixture-of-Experts (MoE) (Shazeer et al. 2017) provides a natural remedy to this simplicity bias by sparsely activating only a small subset of experts for each input, enabling different parameter blocks to specialize in distinct behaviors. As a result, MoE can prevent frequent simple decisions from dominating shared parameters, thereby reserving dedicated capacity for harder sub-skills across trajectories. This motivation aligns with a broad line of MoE research (i.e. (Lepikhin et al. 2021; Du et al. 2022; Zoph et al. 2022)) that scales model capacity efficiently via conditional computation and encourages expert specialization through routing, which has proven effective in large language models and multi-domain learning settings. However, directly adopting conventional MoE for RL-based agent policies is nontrivial: traditional MoE relies on token-level routing that assigns experts independently per token based on local representations, which is mismatched to sequential decision making. As shown in Figure 2(a), such token-level routing induces excessive expert switching (45 step-level equivalent switches per

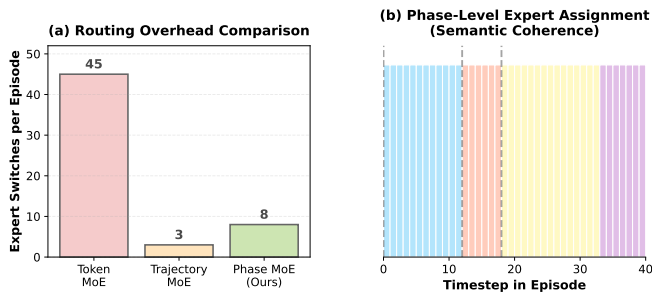


Figure 2: **Routing Granularity Comparison.** (a) Expert switches per episode across routing strategies. Token-level MoE causes excessive fragmentation (45 switches), while trajectory-level MoE is overly coarse (3 switches). PA-MoE strikes a balance with 8 switches per episode. (b) Visualization of phase-level expert assignment showing semantic coherence: the same expert (indicated by color) is maintained within each contiguous behavioral phase, with switches occurring only at phase boundaries.

episode), fragmenting temporally coherent, phase-consistent patterns (e.g., planning, acting, verifying) into scattered expert assignments. Consequently, specialization is weakened and credit assignment is dispersed across experts, thereby undermining the very benefit MoE is expected to provide.

In this paper, we propose **Phase-Aware Mixture of Experts (PA-MoE)**, a phase-aware MoE policy that learns the phase structure of trajectories end-to-end from the RL objective. At its core, PA-MoE introduces a lightweight *phase router* that predicts an expert assignment at the environment-step level and, crucially, enforces temporally consistent routing so that contiguous segments of a trajectory are handled by the same expert. To keep the parameter overhead minimal, each expert is implemented as a LoRA module (Hu et al. 2022) on top of a shared backbone, which isolates phase-specific updates while retaining general language and reasoning capabilities.

This phase-consistent routing has two practical advantages. First, by allowing each expert to accumulate stable learning signals over contiguous segments, it encourages experts to develop distinct behavioral specializations. Consequently, it mitigates simplicity bias by preventing easy behaviors from monopolizing shared parameters. As a result, PA-MoE achieves more balanced expert utilization and more uniform performance across task difficulties, as shown in Figure 1(b). Second, it provides a routing granularity that better matches sequential decision making: token-level routing switches experts excessively, fragmenting temporally coherent behaviors and dispersing credit assignment across experts, whereas trajectory-level routing is overly coarse, limiting within-episode adaptation when the required behavior changes. In contrast, PA-MoE strikes a principled middle ground by reducing unnecessary switching while still permitting expert changes at genuine phase boundaries, thereby balancing coherence and adaptability. As illustrated in Figure 2(b), the same expert is maintained within each contiguous segment, with switches occurring only at semantic phase boundaries, reinforcing consistent strategy execution. Experi-

ments on ALFWorld and WebShop demonstrate that PA-MoE improves over the GiGPO baseline by +7.7% and +14.9% respectively, and notably, PA-MoE with 1.5B parameters outperforms the 7B baseline.

## Related Work

**LLM-Based Agents.** Prompting methods such as ReAct (Yao et al. 2023b), Reflexion (Shinn et al. 2023) and Tree-of-Thoughts (Yao et al. 2023a) enable LLM agents through in-context demonstrations, but are bounded by context length and cannot improve from trial-and-error experience. Supervised fine-tuning approaches including Agent-Tuning (Zeng et al. 2024), FireAct (Chen et al. 2023) and Toolformer (Schick et al. 2023) distill successful trajectories into model weights, achieving better generalization than prompting but requiring curated demonstrations and not optimizing for long-horizon outcomes directly. Reinforcement learning enables agents to improve the policy through environment interaction. Recent work applies policy-gradient methods, i.e. REINFORCE (Williams 1992), PPO (Schulman et al. 2017), GRPO (Shao et al. 2024), and GiGPO (Feng et al. 2025), to train LLM policies on agentic tasks, with RLHF (Ouyang et al. 2022) demonstrating the effectiveness of RL for aligning language models. However, these methods use a single policy network for all behavioral phases, leading to simplicity bias when heterogeneous behaviors induce conflicting learning signals. Gradient-surgery techniques like PC-Grad (Yu et al. 2020) and CAGrad (Liu et al. 2021) mitigate conflicts by projecting or rescaling gradients at each update, but operate at the optimization level and do not induce persistent specialization for temporally contiguous phases within a trajectory. PA-MoE addresses this gap through architectural parameter isolation that persists across training.

**Mixture of Experts.** MoE architectures scale model capacity through sparse expert activation (Shazeer et al. 2017). Switch Transformer (Fedus, Zoph, and Shazeer 2022) simplifies routing to top-1 selection, while Mixtral (Jiang et al. 2024) demonstrates MoE effectiveness in open-weight LLMs. These advances target language modeling, where token-level routing aligns naturally with the next-token prediction objective. For sequential decision-making, this granularity is misaligned: agent trajectories are structured by temporally extended behavioral phases, not linguistic tokens. Token-level routing fragments coherent action sequences, where different tokens within a single “open fridge” action may route to different experts, disrupting behavioral consistency. To our knowledge, no prior work explores phase-level expert routing for agentic tasks. PA-MoE bridges this gap by routing at environment-step granularity with temporal consistency regularization, enabling experts to specialize for distinct behavioral modes.

**Hierarchical and Modular RL.** Hierarchical RL decomposes behavior into temporal abstractions. The options framework (Sutton, Precup, and Singh 1999) introduces temporally extended actions with initiation and termination conditions, while Option-Critic (Bacon, Harb, and Precup 2017) learns options end-to-end. These methods modify the MDP structure by introducing semi-MDPs or hierarchical action

spaces, and often require intrinsic rewards or explicit termination learning. Modular approaches (Andreas, Klein, and Levine 2017; Devin et al. 2017; Goyal et al. 2021) decompose policies into reusable components but typically require predefined module inventories or compositional task structure. PA-MoE is complementary to both lines: we do not alter the action space or introduce temporal action abstractions, applying temporal abstraction solely to parameter routing. Unlike modular policies, we do not require predefined phase categories; the router discovers boundaries that maximize task reward through end-to-end learning driven directly by the RL objective.

## Method

We present Phase-Aware Mixture of Experts (PA-MoE), which decomposes an agent policy into specialized experts operating at the phase level. As shown in Figure 3, PA-MoE consists of a phase-aware router that selects experts based on execution context, and a set of LoRA-based experts sharing a frozen base language model. At each timestep  $t$ , given observation  $o_t$ , action history  $h_t$ , and goal  $g$ , the router selects an expert  $k^*$  which then generates action  $a_t$ . PA-MoE is agnostic to the underlying RL algorithm and can be combined with any policy-gradient method. Intuitively, phase-aware routing reduces policy gradient variance by isolating updates from heterogeneous behavioral phases into disjoint parameters; we provide analysis and empirical validation in Appendix .

### Phase-Aware Router

The router  $\pi_r$  determines which expert handles each decision by integrating two complementary information streams (Figure 3): goal-conditioned observation encoding and temporal history modeling.

**Observation Encoding.** We apply cross-attention between the current observation  $o_t$  and task goal  $g$  to produce a goal-conditioned representation:

$$o_t^{\text{align}} = \text{CrossAttn}(Q=\text{Enc}(o_t), K=\text{Enc}(g), V=\text{Enc}(g)),$$

where  $\text{Enc}(\cdot)$  denotes mean-pooling over the final hidden states of the frozen base model, producing a fixed-dimensional representation  $\in \mathbb{R}^{d_{\text{model}}}$  for variable-length text inputs. This cross-attention mechanism allows the router to focus on goal-relevant aspects of the observation, distinguishing between states that appear similar but require different behavioral modes depending on the task objective.

**Temporal Modeling.** We encode the recent action and observation history  $h_t = [a_{t-L:t-1}, o_{t-L:t-1}]$  using a 3-layer LSTM. Each action and observation in the history is first embedded via mean-pooling over the base model’s token embeddings, then concatenated and fed sequentially:

$$h_t^{\text{enc}} = \text{LSTM}(\text{Embed}(h_t)) \in \mathbb{R}^d, \quad (1)$$

where  $L = 5$  is the history window and  $d = 256$  is the LSTM hidden dimension. The LSTM’s recurrent structure is well-suited for tracking sequential state changes that signal phase transitions in long-horizon trajectories.

**Expert Distribution.** Both representations are concatenated and passed through an MLP to obtain the expert distribution:

$$p_t = \text{softmax}(\text{MLP}([o_t^{\text{align}}; h_t^{\text{enc}}]) / \tau) \in \Delta^K, \quad (2)$$

where  $\tau$  is a temperature parameter (see Section ).

**Expert Selection.** We use deterministic expert selection via  $k^* = \arg \max_k p_t^k$  for both training and inference. The router parameters are optimized through the RL objective as described in Section .

### Temporal Consistency

To encourage temporally stable expert assignments, we introduce a consistency mechanism through two components.

**Switching Penalty.** Let  $z_t = \arg \max_k p_t^k$  denote the selected expert at step  $t$ . We penalize transitions between consecutive steps:

$$\mathcal{L}_{\text{switch}} = \frac{\lambda_s}{T-1} \sum_{t=1}^{T-1} \mathbf{1}[z_t \neq z_{t+1}],$$

where  $\mathbf{1}[\cdot]$  is the indicator function,  $\lambda_s = 0.05$ , and  $T$  denotes the episode length (which varies across episodes). Since the indicator function is non-differentiable, we implement the backward pass using a differentiable surrogate: we replace  $\mathbf{1}[z_t \neq z_{t+1}]$  with  $1 - \sum_k p_t^k \cdot p_{t+1}^k$  during gradient computation, which measures the soft disagreement between consecutive routing distributions. The forward pass uses the hard indicator for accurate loss computation, while the backward pass uses this soft approximation to propagate gradients to router parameters.

**Temperature Annealing.** We apply temperature annealing to the router’s softmax during training following a linear schedule:

$$\tau(t) = \max\left(\tau_f, \tau_0 - \frac{(\tau_0 - \tau_f) \cdot t}{T_{\text{anneal}}}\right), \quad (3)$$

with  $\tau_0 = 2.0$ ,  $\tau_f = 0.5$ , and  $T_{\text{anneal}} = 3000$  steps. High initial temperature encourages exploration of different routing patterns, while low final temperature produces more decisive assignments.

**Switch Metric.** We define an expert switch as a change in the selected expert between consecutive environment steps:  $\mathbf{1}[z_t \neq z_{t+1}]$  where  $z_t = \arg \max_k p_t^k$ . This step-level metric directly measures behavioral coherence. Fewer switches indicate that the same expert handles temporally contiguous decisions, enabling consistent strategy execution within each phase. This differs from token-level switches (which would count routing changes during action generation); we use step-level switches because agent behavior is structured by environment interactions, not linguistic tokenization.

Combined, these mechanisms reduce expert switches from 45 per episode (without consistency) to 8.4 (with consistency), while maintaining the flexibility to adapt at genuine phase boundaries. For reference, token-level MoE exhibits approximately 1,200 routing changes per episode when measured at token granularity; we report the step-level equivalent (45 environment steps with at least one intra-step expert change) for comparable measurement across methods. See Appendix for details on the token-level baseline and metric conversion.

### Behavioral Experts

We implement  $K = 4$  experts as LoRA adapters (Hu et al. 2022) sharing a frozen base model  $\theta_{\text{base}}$  (Figure 3). Each

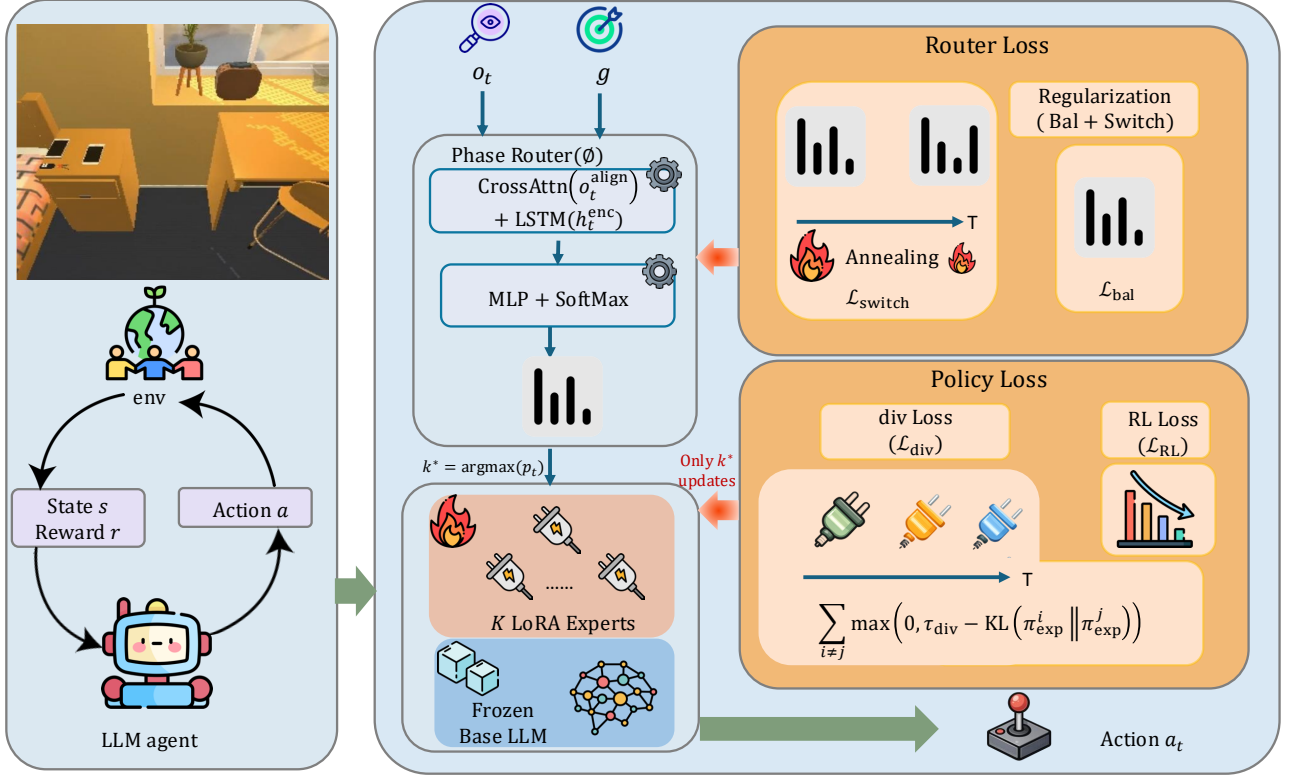


Figure 3: **PA-MoE Architecture.** **Upper panel:** Phase-Aware Router (Sec. ) processes observation  $o_t$  and goal  $g$  via cross-attention, and action history  $h_t$  via LSTM, to select expert  $k^* = \arg \max p_i$ . Balance loss  $\mathcal{L}_{\text{bal}}$  ensures uniform expert utilization. **Lower panel:** Phase-Aware MoE Execution shows agent-environment interaction. The router selects expert  $k^*$  from  $K$  LoRA-based experts sharing a frozen base model (gray). The selected expert generates action via policy  $\pi_{\text{exp}}^{k^*}(a_t|s_t, h_t, g)$ . Training optimizes both router and experts jointly via RL loss  $\mathcal{L}_{\text{RL}}$  and diversity loss  $\mathcal{L}_{\text{div}}$  (Sec. ).

expert  $k$  is parameterized as:

$$\pi_{\text{exp}}^k(a|s) = \text{LLM}(a|s; \theta_{\text{base}} + B_k A_k), \quad (4)$$

where  $B_k \in \mathbb{R}^{d \times r}$  and  $A_k \in \mathbb{R}^{r \times d}$  are low-rank matrices with rank  $r = 32$ , applied to query and value projections across all transformer layers.

LoRA experts share a frozen backbone, providing parameter efficiency while maintaining general language capabilities. The low-rank constraint encourages complementary adjustments to the base policy. Expert specialization emerges during training without manual assignment. Phase-specific entropy demands differ sharply across behavioral modes; we provide quantitative entropy analysis in Appendix .

### Behavioral Phase Definition

PA-MoE operates at the phase level rather than token or trajectory level. We formally define:

**Definition 0.1** (Behavioral Phase). A behavioral phase  $\phi$  is a maximal trajectory segment  $[t_{\text{start}}, t_{\text{end}}]$  where the router assigns the same expert:  $\arg \max_k \pi_r(s_t)^k = k^*$  for all  $t \in \phi$ .

**Post-hoc Validation.** We verify that learned phases exhibit behavioral coherence by measuring within-phase entropy

variance. Empirically, phases satisfy  $\text{Var}_{t \in \phi}[H(\pi(a|s_t))] < 0.18 \text{ bits}^2$ . Phase boundaries occur when task requirements change, triggering both expert switches and entropy shifts.

### Policy-Gradient Integration and Optimization

PA-MoE integrates with any policy-gradient method. The training procedure consists of two components: (1) the router determines expert assignments based on execution context, and (2) the selected expert is optimized using the base algorithm’s update rule.

**General Framework.** At each timestep  $t$ , the router selects expert  $k^* = \arg \max_k \pi_r(k|s_t)$ . The selected expert  $\pi_{\text{exp}}^{k^*}$  generates action  $a_t$  and receives the policy gradient update from the base RL algorithm. Only the selected expert receives gradients at each step, enabling phase-level parameter isolation.

**Instantiations.** In our primary experiments, we instantiate PA-MoE with GiGPO (Feng et al. 2025), which computes group-based advantages from multiple sampled trajectories. For each state  $s$ , we sample  $n = 8$  trajectories and compute advantages:

$$A_t^{\text{group}} = f(\text{rank}(\tau), R(\tau)), \quad (5)$$

based on relative trajectory rankings within each group. The

selected expert is updated via the clipped surrogate objective:

$$\mathcal{L}_{\text{RL}}^{k^*} = \mathbb{E}_t \left[ \min \left( \rho_t A_t^{\text{group}}, \text{clip}(\rho_t, 1-\epsilon, 1+\epsilon) A_t^{\text{group}} \right) \right],$$

where  $\rho_t = \pi_{\text{exp}}^{k^*}(a_t|s_t) / \pi_{\text{exp,old}}^{k^*}(a_t|s_t)$  is the importance sampling ratio and  $\epsilon = 0.2$  is the clipping threshold.

**Router Optimization.** The router is trained jointly with the experts through the same RL objective. Specifically, the router parameters  $\theta_r$  receive gradients from the policy loss of the selected expert. Since expert selection is deterministic ( $k^* = \arg \max_k p_t^k$ ), we use the straight-through estimator (Bengio, Léonard, and Courville 2013) to propagate gradients: the forward pass uses hard expert selection, while the backward pass computes gradients with respect to  $p_t$  as if the selection were soft. This allows the router to learn which expert assignments lead to higher group-relative advantages.

**Generalization to Other Algorithms.** PA-MoE can also be applied to other RL policy-gradient methods by substituting the appropriate advantage computation and policy objective. For PPO, we use the standard generalized advantage estimator (GAE) (Schulman et al. 2016) with a shared critic network. For GRPO, we employ group-relative policy optimization with ranking-based advantages. For RLOO, we use leave-one-out baseline estimation. The router-expert interaction mechanism remains identical across all instantiations.

**Regularization.** To prevent degenerate solutions, we employ two regularization terms. The diversity loss enforces minimum separation between expert policies:

$$\mathcal{L}_{\text{div}} = \sum_{i \neq j} \max(0, \tau_{\text{div}} - \text{KL}(\pi_{\text{exp}}^i \| \pi_{\text{exp}}^j)), \quad (6)$$

with margin  $\tau_{\text{div}} = 0.1$ . To avoid the computational cost of  $K(K-1)$  forward passes, we compute  $\mathcal{L}_{\text{div}}$  periodically (every 100 training steps) using cached action distributions from recent trajectories. Specifically, we maintain a buffer of the most recent 1,000 state-action pairs per expert; at each diversity update, we sample 64 states and compute KL divergences using the cached logits with current expert parameters. During diversity loss computation, gradients flow only to expert parameters while the router remains detached.

The balance loss:

$$\mathcal{L}_{\text{bal}} = \sum_{k=1}^K (f_k - 1/K)^2, \quad (7)$$

where  $f_k$  is expert  $k$ 's activation frequency over a training batch, prevents router collapse by encouraging uniform utilization.

The complete objective combines the base RL loss with regularization:

$$\mathcal{L} = \mathcal{L}_{\text{RL}} + \alpha \mathcal{L}_{\text{div}} + \beta \mathcal{L}_{\text{bal}} + \gamma \mathcal{L}_{\text{switch}} \quad (8)$$

Here  $\mathcal{L}_{\text{RL}}$  denotes the policy objective of the base algorithm (e.g., GiGPO, PPO, GRPO, or RLOO).

## Experiments

### Experimental Setup

**Benchmark datasets.** We evaluate our PA-MoE on ALF-World (Shridhar et al. 2021), a household task benchmark requiring multi-step interaction, and WebShop (Yao et al.

2022), a goal-directed web navigation environment. ALF-World contains six task types involving object manipulation; we train on approximately 3,500 procedurally generated tasks and evaluate on 140 held-out validation instances, with success measured as task completion within 50 steps. WebShop simulates e-commerce where agents search for and purchase products matching natural language specifications across 500 validation tasks; we report both score (weighted attribute matching) and binary success rate.

We experiment with Qwen2.5-1.5B-Instruct and Qwen2.5-7B-Instruct (Yang et al. 2024) as base models. Baselines include prompt-based methods (vanilla prompting, ReAct (Yao et al. 2023b), Reflexion (Shinn et al. 2023)) and RL-trained policies using PPO (Schulman et al. 2017), RLOO (Ahmadian et al. 2024), GRPO (Shao et al. 2024), GiGPO (Feng et al. 2025), and GEPO (Yuan et al. 2025). For closed-source models, we report GPT-4o and Gemini-2.5-Pro results from prior work (Feng et al. 2025).

Our PA-MoE uses  $K = 4$  experts with LoRA rank  $r = 32$  applied to query and value projections. We set the  $\alpha = 0.01$ ,  $\beta = 0.001$  and  $\gamma = 1$  respectively. We use 8 H800 GPUs for all experiments.

### Main Results

Table 1 reports comprehensive comparisons across model sizes, RL algorithms, and benchmarks.

**ALFWorld Performance.** PA-MoE+GiGPO with Qwen2.5-1.5B achieves 93.8% overall success, improving over the GiGPO baseline (86.1%) by +7.7 percentage points. Gains concentrate on tasks requiring precise multi-step manipulation. For example, heating reaches 100% (vs. 91.3%), cooling 89.5% (vs. 71.7%), and cleaning 95.8% (vs. 91.8%). These tasks involve low-frequency but decisive actions, which is exactly where simplicity bias most severely impacts baselines. Taken together, the improvement pattern reveals PA-MoE’s mechanism. Navigation-heavy tasks (pick, pick2) show modest gains (+1.1%, +12.2%) since baselines already allocate sufficient capacity to frequent actions. Manipulation-heavy tasks show larger gains (+8.7% heating, +17.8% cooling) because PA-MoE dedicates Expert 2 to these critical but rare interactions. This asymmetric improvement directly reflects the capacity rebalancing shown in Section .

**Cross-Algorithm Generalization.** PA-MoE improves all tested RL algorithms, confirming that benefits stem from architectural design rather than algorithm-specific interactions: With GRPO, overall accuracy increases from 72.8% to 74.2%, while the most challenging task type (look-at-object) jumps dramatically from 53.7% to 87.5% (a 33.8 percentage point improvement). RLOO shows the largest overall gain at 4.5 points (69.7%  $\rightarrow$  74.2%), with substantial improvements on manipulation tasks such as Clean (+16.5%) and Heat (+20.5%), though with some regression on simpler Pick tasks. Even PPO, whose separate critic network already provides some degree of gradient separation, achieves modest but consistent improvement (54.4%  $\rightarrow$  56.2%). The varying improvement magnitudes correlate with baseline headroom: weaker baselines (GRPO, RLOO) benefit more from capacity reallocation than stronger ones (GiGPO).

Table 1: Performance comparison on ALFWorld and WebShop benchmarks. For ALFWorld, we report the average success rate (%) for each subtask as well as the overall result. For WebShop, we report both the average score and the average success rate (%). We report mean and standard deviation over 3 random seeds for RL methods. Prompting results are deterministic single runs. “GiGPO w/o std” refers to variants without advantage standardization, respectively.

Type	Method	ALFWorld						WebShop		
		Pick	Look	Clean	Heat	Cool	Pick2	All	Score	Succ.
<b>Closed-Source Model<sup>‡</sup></b>										
Prompting	GPT-4o <sup>†</sup>	75.3	60.8	31.2	56.7	21.6	49.8	48.0	31.8	23.7
Prompting	Gemini-2.5-Pro <sup>†</sup>	92.8	63.3	62.1	69.0	25.4	58.7	60.3	42.5	35.9
<b>Qwen2.5-1.5B-Instruct</b>										
Prompting	Qwen2.5 <sup>†</sup>	5.9	5.5	3.3	9.7	4.2	0.0	4.1	23.1	5.2
Prompting	ReAct <sup>†</sup>	17.4	20.5	15.7	6.2	7.7	2.0	12.8	40.1	11.3
Prompting	Reflexion <sup>†</sup>	35.3	22.2	21.7	13.6	19.4	3.7	21.8	55.8	21.9
RL Training	GEPO	98.7 $\pm$ 1.2	79.9 $\pm$ 5.9	94.6 $\pm$ 2.3	81.9 $\pm$ 9.0	76.6 $\pm$ 9.1	88.6 $\pm$ 4.8	89.1 $\pm$ 0.8	89.9 $\pm$ 1.4	75.6 $\pm$ 2.5
RL Training	PPO	64.8 $\pm$ 3.5	40.5 $\pm$ 6.9	57.1 $\pm$ 4.9	60.6 $\pm$ 6.6	46.4 $\pm$ 4.0	47.4 $\pm$ 1.9	54.4 $\pm$ 3.1	73.8 $\pm$ 3.0	51.5 $\pm$ 2.9
RL Training	<b>PPO + PA-MoE</b>	<b>88.6<math>\pm</math>3.4</b>	<b>37.5<math>\pm</math>6.2</b>	<b>50.0<math>\pm</math>4.4</b>	<b>55.6<math>\pm</math>6.0</b>	<b>36.8<math>\pm</math>4.4</b>	<b>37.5<math>\pm</math>1.1</b>	<b>56.2<math>\pm</math>3.4</b>	<b>73.9<math>\pm</math>3.4</b>	<b>52.3<math>\pm</math>2.4</b>
RL Training	RLOO	88.3 $\pm$ 3.0	52.8 $\pm$ 8.6	71.0 $\pm$ 5.9	62.8 $\pm$ 8.7	66.4 $\pm$ 5.5	56.9 $\pm$ 4.7	69.7 $\pm$ 2.5	73.9 $\pm$ 5.6	52.1 $\pm$ 6.7
RL Training	<b>RLOO + PA-MoE</b>	<b>74.3<math>\pm</math>3.4</b>	<b>50.0<math>\pm</math>7.2</b>	<b>87.5<math>\pm</math>6.4</b>	<b>83.3<math>\pm</math>8.0</b>	<b>73.7<math>\pm</math>5.4</b>	<b>62.5<math>\pm</math>4.1</b>	<b>74.2<math>\pm</math>2.4</b>	<b>73.9<math>\pm</math>5.4</b>	<b>58.6<math>\pm</math>6.4</b>
RL Training	GRPO	85.3 $\pm$ 1.5	53.7 $\pm$ 8.0	84.5 $\pm$ 6.8	78.2 $\pm$ 7.9	59.7 $\pm$ 5.0	53.5 $\pm$ 5.6	72.8 $\pm$ 3.6	75.8 $\pm$ 3.5	56.8 $\pm$ 3.8
RL Training	<b>GRPO + PA-MoE</b>	<b>87.5<math>\pm</math>1.4</b>	<b>87.5<math>\pm</math>6.2</b>	<b>87.5<math>\pm</math>6.4</b>	<b>81.2<math>\pm</math>7.2</b>	<b>50.0<math>\pm</math>5.4</b>	<b>45.8<math>\pm</math>5.1</b>	<b>74.2<math>\pm</math>3.4</b>	<b>73.9<math>\pm</math>3.4</b>	<b>57.0<math>\pm</math>3.4</b>
RL Training	GiGPO	94.4 $\pm$ 5.9	67.5 $\pm$ 3.6	94.8 $\pm$ 3.8	94.4 $\pm$ 3.8	79.8 $\pm$ 4.7	76.4 $\pm$ 5.4	86.7 $\pm$ 1.7	83.1 $\pm$ 1.6	65.0 $\pm$ 3.2
RL Training	GiGPO w/o std	96.0 $\pm$ 1.4	76.5 $\pm$ 3.9	91.8 $\pm$ 5.5	91.3 $\pm$ 6.3	71.7 $\pm$ 8.4	79.5 $\pm$ 7.7	86.1 $\pm$ 4.7	83.5 $\pm$ 1.8	67.4 $\pm$ 4.5
RL Training	<b>GiGPO + PA-MoE</b>	<b>97.1<math>\pm</math>1.4</b>	<b>75.0<math>\pm</math>3.2</b>	<b>95.8<math>\pm</math>6.4</b>	<b>100.0<math>\pm</math>0.0</b>	<b>89.5<math>\pm</math>4.4</b>	<b>91.7<math>\pm</math>4.1</b>	<b>93.8<math>\pm</math>2.4</b>	<b>91.0<math>\pm</math>1.4</b>	<b>82.3<math>\pm</math>3.4</b>
<b>Qwen2.5-7B-Instruct</b>										
Prompting	Qwen2.5 <sup>†</sup>	33.4	21.6	19.3	6.9	2.8	3.2	14.8	26.4	7.8
Prompting	ReAct <sup>†</sup>	48.5	35.4	34.3	13.2	18.2	17.6	31.2	46.2	19.5
Prompting	Reflexion <sup>†</sup>	62.0	41.6	44.9	30.9	36.3	23.8	42.7	58.1	28.8
RL Training	GEPO	100.0 $\pm$ 0.0	80.2 $\pm$ 9.2	98.6 $\pm$ 2.4	95.6 $\pm$ 4.0	94.3 $\pm$ 5.9	86.7 $\pm$ 12.6	94.9 $\pm$ 3.8	91.0 $\pm$ 2.7	80.5 $\pm$ 6.7
RL Training	PPO	92.3 $\pm$ 4.0	64.0 $\pm$ 8.4	92.5 $\pm$ 2.4	89.5 $\pm$ 7.0	80.3 $\pm$ 2.0	68.8 $\pm$ 8.3	80.4 $\pm$ 2.7	81.4 $\pm$ 3.1	68.7 $\pm$ 5.1
RL Training	<b>PPO + PA-MoE</b>	<b>93.5<math>\pm</math>3.8</b>	<b>67.5<math>\pm</math>7.6</b>	<b>93.8<math>\pm</math>2.2</b>	<b>91.2<math>\pm</math>6.4</b>	<b>82.5<math>\pm</math>2.4</b>	<b>71.5<math>\pm</math>7.8</b>	<b>82.6<math>\pm</math>2.5</b>	<b>82.8<math>\pm</math>2.9</b>	<b>70.3<math>\pm</math>4.8</b>
RL Training	RLOO	87.6 $\pm$ 4.3	78.2 $\pm$ 8.3	87.3 $\pm$ 5.8	81.3 $\pm$ 7.6	71.9 $\pm$ 5.2	48.9 $\pm$ 8.4	75.5 $\pm$ 4.6	80.3 $\pm$ 3.2	65.7 $\pm$ 4.0
RL Training	<b>RLOO + PA-MoE</b>	<b>89.2<math>\pm</math>4.0</b>	<b>80.5<math>\pm</math>7.9</b>	<b>89.5<math>\pm</math>5.4</b>	<b>83.5<math>\pm</math>7.2</b>	<b>74.2<math>\pm</math>5.0</b>	<b>52.5<math>\pm</math>8.0</b>	<b>78.2<math>\pm</math>4.2</b>	<b>82.1<math>\pm</math>3.0</b>	<b>67.8<math>\pm</math>3.8</b>
RL Training	GRPO	90.8 $\pm$ 5.1	66.1 $\pm$ 6.7	89.3 $\pm$ 5.4	74.7 $\pm$ 6.9	72.5 $\pm$ 5.4	64.7 $\pm$ 7.3	77.6 $\pm$ 5.2	79.3 $\pm$ 2.8	66.1 $\pm$ 3.7
RL Training	<b>GRPO + PA-MoE</b>	<b>92.3<math>\pm</math>4.6</b>	<b>69.5<math>\pm</math>6.4</b>	<b>91.5<math>\pm</math>5.0</b>	<b>77.5<math>\pm</math>6.5</b>	<b>75.0<math>\pm</math>5.2</b>	<b>67.8<math>\pm</math>7.0</b>	<b>80.2<math>\pm</math>4.8</b>	<b>81.5<math>\pm</math>2.6</b>	<b>68.5<math>\pm</math>3.5</b>
RL Training	GiGPO	97.7 $\pm$ 1.6	82.7 $\pm$ 7.9	98.8 $\pm$ 1.6	83.7 $\pm$ 7.2	89.3 $\pm$ 5.2	79.2 $\pm$ 6.6	90.8 $\pm$ 1.3	84.4 $\pm$ 2.9	72.8 $\pm$ 3.2
RL Training	GiGPO w/o std	91.8 $\pm$ 5.4	88.6 $\pm$ 6.3	95.9 $\pm$ 3.2	90.2 $\pm$ 2.6	86.5 $\pm$ 5.5	85.2 $\pm$ 4.7	90.2 $\pm$ 2.3	86.2 $\pm$ 2.6	75.2 $\pm$ 3.8
RL Training	<b>GiGPO + PA-MoE</b>	<b>87.5<math>\pm</math>1.6</b>	<b>100.0<math>\pm</math>0.0</b>	<b>100.0<math>\pm</math>0.0</b>	<b>100.0<math>\pm</math>0.0</b>	<b>100.0<math>\pm</math>0.0</b>	<b>100.0<math>\pm</math>0.0</b>	<b>95.3<math>\pm</math>0.8</b>	<b>93.1<math>\pm</math>1.4</b>	<b>82.8<math>\pm</math>3.4</b>

**Parameter Efficiency.** PA-MoE (93.8%) with 1.5B parameters outperforms the vanilla 7B GiGPO baseline (90.2%) by +3.6 points while using fewer parameters. This demonstrates that architectural design can substitute for parameter scaling when the core bottleneck is capacity allocation rather than raw model capacity. With the 7B model, PA-MoE+GiGPO reaches 95.3% with 100% success on five of six task categories. Compared to GEPO (94.9%), PA-MoE shows comparable performance with substantially lower variance (std 0.8 vs. 3.8), indicating more stable training dynamics.

**WebShop Performance.** PA-MoE+GiGPO achieves 82.3% success and 91.0 score, outperforming GiGPO (67.4%, 83.5) by +14.9 percentage points. The larger gain on WebShop compared to ALFWorld (+14.9 vs. +7.7) reflects WebShop’s longer episodes and more diverse action space, which amplify simplicity bias in baselines. Notably, the 7B model only marginally exceeds 1.5B (82.3%), suggesting that Web-

Shop’s difficulty stems from behavioral diversity rather than language understanding, a bottleneck that parameter scaling alone cannot address but phase-aware routing can.

**Per-Task Variance.** While PA-MoE improves aggregate performance across all algorithm-benchmark pairs, we observe occasional task-specific regressions in some configurations, particularly with PPO and RLOO where baseline performance is already low and training is less stable. These regressions are concentrated in a small subset of tasks and do not change the overall ranking. We provide detailed analysis in Appendix .

## Ablation Studies

We conduct systematic ablations using Qwen2.5-1.5B with GiGPO on ALFWorld. All ablation results report mean over 3 seeds; standard deviations are provided in Appendix .

**Number of Experts.** Table 2 compares expert counts. The

Table 2: Ablation on number of experts ( $K$ ).  $K=0$  uses a single shared LoRA adapter without routing. All six ALFWorld task types shown. Bold indicates best per column; underline indicates ties with best. We report the average success rate (%) for each subtask as well as the overall result. See Appendix for  $K=3, 5$  results and standard deviations.

$K$	Pick	Pick2	Look	Heat	Cool	Clean	All
0	94.3	87.5	62.5	94.4	<b>89.5</b>	83.3	88.3
2	<u>97.1</u>	<u>91.7</u>	62.5	<b>100.0</b>	73.7	<b>100.0</b>	91.4
4 (ours)	<b>97.1</b>	<b>91.7</b>	<b>75.0</b>	<b>100.0</b>	<b>89.5</b>	95.8	<b>93.8</b>
6	91.4	70.8	62.5	<b>100.0</b>	84.2	91.7	85.9

Table 3: Comparison of routing granularities. Switches denotes average expert switches per episode, measured at the environment step level (i.e.,  $\sum_t \mathbf{1}[z_t \neq z_{t+1}]$ ). Trajectory-level assigns one expert per episode at  $t=0$  based on initial observation, with minimal within-episode adaptation. See Appendix for token-level baseline details.

Routing	Pick(%)	Heat(%)	All(%)
Token-level	88.6	86.1	85.7
Trajectory-level	94.3	91.7	88.5
Phase-level (ours)	<b>97.1</b>	<b>100.0</b>	<b>93.8</b>

$K = 0$  configuration uses a single shared LoRA adapter without phase-aware routing, and all decisions use the same expert regardless of behavioral context. This achieves 88.3% success, already +2.2 points over vanilla GiGPO (86.1%), indicating that LoRA adaptation provides some benefit even without routing. However, performance remains uneven: 94.4% on heating versus 62.5% on look-at-object, a 32-point gap.

Adding  $K = 2$  experts improves to 91.4%, though look-at-object remains unchanged.  $K = 4$  achieves our best result at 93.8%, with more balanced performance across tasks. The total improvement (+7.7%) can be attributed to two sources: LoRA adaptation (+2.2%, comparing  $K=0$  to vanilla GiGPO) and phase-aware multi-expert specialization (+5.5%, comparing  $K=4$  to  $K=0$ ).  $K = 6$  degrades to 85.9% due to data fragmentation: with approximately 3,500 training tasks across 6 task types and 6 experts, finer expert partitioning reduces per-expert sample efficiency. We use  $K = 4$  experts; performance is robust across  $K \in \{3, 4, 5\}$  as detailed in Appendix .

**Routing Granularity.** Table 3 compares temporal scales. Token-level routing causes severe fragmentation (45 step-level switches/episode), yielding only 85.7% success, which is 8.1 points below phase-level. The gap is pronounced on manipulation tasks (86.1% vs. 100.0% on heating) where multi-step sequences require coherence. Trajectory-level routing (3 switches; primarily using a single expert per episode with limited adaptation) achieves 88.5% but lacks fine-grained within-episode flexibility.

**Router Components.** Table 4 ablates router inputs. Removing action history drops performance to 89.2% (-4.6), as the router loses context about task progress. Removing goal attention yields 90.5% (-3.3), preventing appropriate phase

Table 4: Ablation on router components.

Router Configuration	Success Rate (%)
w/o action history	89.2
w/o goal attention	90.5
w/o both	86.8
Full router (ours)	<b>93.8</b>

Table 5: Emergent expert specialization on ALFWorld (role and activation frequency).

	E1	E2	E3	E4
Role	Explore	Manipulate	Navigate	Recover
Action (%)	73	82	64	71

selection. Without both, performance falls to 86.8%, barely exceeding baseline.

**Regularization Terms.** Removing  $\mathcal{L}_{\text{div}}$  causes expert collapse (88.3%), while removing  $\mathcal{L}_{\text{bal}}$  leads to router collapse (87.5%). Both regularizers are necessary; see Appendix for details.

**Comparison with Gradient Surgery Methods.** Prior work addresses gradient conflicts through local modifications at each update step (PCGrad (Yu et al. 2020), GradNorm (Chen et al. 2018)). We compare PA-MoE against these baselines by applying gradient surgery to phase-partitioned losses. As detailed in Appendix , gradient surgery provides modest gains over GiGPO baseline (+0.7-1.8%) but falls substantially short of PA-MoE’s +7.7% improvement. PA-MoE provides persistent parameter separation across phases, while gradient-level approaches modify updates at each step without preventing heterogeneous phases from repeatedly competing for shared parameters over long horizons.

### Effectiveness of Phase-Aware Routing

We verify that the phase-aware routing of our PA-MOE produces meaningful expert specialization.

**Expert Specialization Patterns.** We analyze expert activation patterns across 500 validation episodes. Table 5 summarizes the emergent specialization in terms of role and activation frequency. Quantitative entropy statistics are reported in Appendix .

**Phase Semantic Grounding.** To verify that learned phases correspond to interpretable behavioral modes, we compare router assignments against human annotations. Three annotators labeled 50 episodes with phase boundaries (inter-annotator  $\kappa = 0.83$ ). Router-assigned phases achieve 87% step-level overlap with human labels, with disagreements concentrated at ambiguous phase boundaries. We observe a substantial entropy gap between exploration and interaction; quantitative results are reported in Appendix .

## Conclusion

We identified a fundamental mismatch between single-policy networks and the heterogeneous demands of agentic tasks, where simplicity bias, gradient conflicts, and mode mismatch

cause performance disparities across task types. PA-MoE addresses these issues through LoRA adaptation and phase-aware multi-expert specialization. PA-MoE achieves 93.8% on ALFWorld (vs. 86.1% baseline) and 82.3% on WebShop (vs. 67.4%), matching or exceeding larger models. Our ablations show phase-level routing is essential: token-level routing causes 8.1% performance loss through fragmentation, while trajectory-level sacrifices adaptability. Analysis reveals emergent expert specialization aligned with intuitive behavioral phases despite no explicit supervision. Comparisons with gradient surgery methods (Appendix ) confirm that persistent parameter isolation yields stronger gains than per-step gradient corrections.

**Limitations and Future Work.** Expert count  $K$  requires task-specific tuning, though performance is robust across  $K \in \{3, 4, 5\}$ . Our experiments focus on discrete actions; continuous control may require modified expert parameterization. The router adds minimal inference overhead, but real-time applications may benefit from router distillation. Whether learned routing patterns transfer across task distributions remains an important direction for future work; preliminary analysis suggests phase boundaries may generalize within task families but require adaptation across domains. Integrating PA-MoE with hierarchical action abstractions could further improve sample efficiency on tasks with deeper temporal structure.

## References

- Ahmadian, A.; Cremer, C.; Gallé, M.; Fadaee, M.; Kreutzer, J.; Pietquin, O.; Üstün, A.; and Hooker, S. 2024. Back to basics: Revisiting reinforce style optimization for learning from human feedback in llms. In *ACL*.
- Andreas, J.; Klein, D.; and Levine, S. 2017. Modular multi-task reinforcement learning with policy sketches. In *International Conference on Machine Learning*, 166–175. PMLR.
- Bacon, P.-L.; Harb, J.; and Precup, D. 2017. The option-critic architecture. In *Proceedings of the Thirty-First AAAI Conference on Artificial Intelligence, AAAI’17*, 1726–1734. AAAI Press.
- Bengio, Y.; Léonard, N.; and Courville, A. C. 2013. Estimating or Propagating Gradients Through Stochastic Neurons for Conditional Computation. *CoRR*, abs/1308.3432.
- Chen, B.; Shu, C.; Shareghi, E.; Collier, N.; Narasimhan, K.; and Yao, S. 2023. FireAct: Toward Language Agent Fine-tuning. *CoRR*, abs/2310.05915.
- Chen, Z.; Badrinarayanan, V.; Lee, C.-Y.; and Rabinovich, A. 2018. GradNorm: Gradient Normalization for Adaptive Loss Balancing in Deep Multitask Networks. In *International Conference on Machine Learning*.
- Devin, C.; Gupta, A.; Darrell, T.; Abbeel, P.; and Levine, S. 2017. Learning modular neural network policies for multi-task and multi-robot transfer. In *International Conference on Robotics and Automation*.
- Du, N.; Huang, Y.; Dai, A. M.; Tong, S.; Lepikhin, D.; Xu, Y.; Krikun, M.; Zhou, Y.; Yu, A. W.; Firat, O.; et al. 2022. GLaM: Efficient Scaling of Language Models with Mixture-of-Experts. In *International Conference on Machine Learning*.
- Fedus, W.; Zoph, B.; and Shazeer, N. 2022. Switch transformers: Scaling to trillion parameter models with simple and efficient sparsity. *Journal of Machine Learning Research*, 23(120): 1–39.
- Feng, L.; Xue, Z.; Liu, T.; and An, B. 2025. Group-in-Group Policy Optimization for LLM Agent Training. In *Advances in Neural Information Processing Systems*.
- Goyal, A.; Lamb, A.; Hoffmann, J.; Sodhani, S.; Levine, S.; Bengio, Y.; and Schölkopf, B. 2021. Recurrent independent mechanisms. In *International Conference on Learning Representations*.
- Hu, E. J.; Shen, Y.; Wallis, P.; Allen-Zhu, Z.; Li, Y.; Wang, S.; Wang, L.; and Chen, W. 2022. LoRA: Low-rank adaptation of large language models. In *International Conference on Learning Representations*.
- Jiang, A. Q.; Sablayrolles, A.; Roux, A.; Mensch, A.; Savary, B.; Bamford, C.; Chaplot, D. S.; de Las Casas, D.; Hanna, E. B.; Bressand, F.; Lengyel, G.; Bour, G.; Lample, G.; Lavaud, L. R.; Saulnier, L.; Lachaux, M.; Stock, P.; Subramanian, S.; Yang, S.; Antoniak, S.; Scao, T. L.; Gervet, T.; Lavril, T.; Wang, T.; Lacroix, T.; and Sayed, W. E. 2024. Mixtral of Experts. *CoRR*, abs/2401.04088.
- Lepikhin, D.; Lee, H.; Xu, Y.; Chen, D.; Firat, O.; Huang, Y.; Krikun, M.; Shazeer, N.; and Chen, Z. 2021. GShard: Scaling Giant Models with Conditional Computation and Automatic Sharding. In *International Conference on Learning Representations*.
- Li, Y.; Yang, Z.; Huang, Y.; Liu, X.; and Qi, G. 2025. C<sup>3</sup>TG: Conflict-aware, Composite, and Collaborative Controlled Text Generation. *arXiv preprint arXiv:2511.09292*.
- Li, Y.; Zhang, S.; Wu, R.; Huang, X.; Chen, Y.; Xu, W.; Qi, G.; and Min, D. 2024. MATEval: a multi-agent discussion framework for advancing open-ended text evaluation. In *International Conference on Database Systems for Advanced Applications*, 415–426. Springer.
- Liu, B.; Liu, X.; Jin, X.; Stone, P.; and Liu, Q. 2021. Conflict-Averse Gradient Descent for Multi-task learning. In *Advances in Neural Information Processing Systems*.
- Ouyang, L.; Wu, J.; Jiang, X.; Almeida, D.; Wainwright, C.; Mishkin, P.; Zhang, C.; Agarwal, S.; Slama, K.; Ray, A.; et al. 2022. Training language models to follow instructions with human feedback. In *Advances in Neural Information Processing Systems*.
- Schick, T.; Dwivedi-Yu, J.; Dessì, R.; Raileanu, R.; Lomeli, M.; Hambro, E.; Zettlemoyer, L.; Cancedda, N.; and Scialom, T. 2023. Toolformer: Language models can teach themselves to use tools. In *Advances in Neural Information Processing Systems*.
- Schulman, J.; Moritz, P.; Levine, S.; Jordan, M. I.; and Abbeel, P. 2016. High-Dimensional Continuous Control Using Generalized Advantage Estimation. In Bengio, Y.; and LeCun, Y., eds., *4th International Conference on Learning Representations*.
- Schulman, J.; Wolski, F.; Dhariwal, P.; Radford, A.; and Klimov, O. 2017. Proximal policy optimization algorithms. *arXiv preprint arXiv:1707.06347*.

- Shao, Z.; Wang, P.; Zhu, Q.; Xu, R.; Song, J.; Zhang, M.; Li, Y.; Wu, Y.; and Guo, D. 2024. DeepSeekMath: Pushing the limits of mathematical reasoning in open language models. *arXiv preprint arXiv:2402.03300*.
- Shazeer, N.; Mirhoseini, A.; Maziarz, K.; Davis, A.; Le, Q. V.; Hinton, G. E.; and Dean, J. 2017. Outrageously Large Neural Networks: The Sparsely-Gated Mixture-of-Experts Layer. In *5th International Conference on Learning Representations*.
- Shinn, N.; Cassano, F.; Gopinath, A.; Narasimhan, K.; and Yao, S. 2023. Reflexion: Language agents with verbal reinforcement learning. In *Advances in Neural Information Processing Systems*.
- Shridhar, M.; Yuan, X.; Côté, M.-A.; Bisk, Y.; Trischler, A.; and Hausknecht, M. 2021. ALFWorld: Aligning Text and Embodied Environments for Interactive Learning. In *International Conference on Learning Representations*.
- Sutton, R. S.; Precup, D.; and Singh, S. 1999. Between MDPs and Semi-MDPs: A Framework for Temporal Abstraction in Reinforcement Learning. *Artif. Intell.*, 112(1-2): 181–211.
- Williams, R. J. 1992. Simple statistical gradient-following algorithms for connectionist reinforcement learning. *Machine Learning*, 8(3): 229–256.
- Yang, A.; Yang, B.; Zhang, B.; Hui, B.; Zheng, B.; Yu, B.; Li, C.; Liu, D.; Huang, F.; Wei, H.; Lin, H.; Yang, J.; Tu, J.; Zhang, J.; Yang, J.; Yang, J.; Zhou, J.; Lin, J.; Dang, K.; Lu, K.; Bao, K.; Yang, K.; Yu, L.; Li, M.; Xue, M.; Zhang, P.; Zhu, Q.; Men, R.; Lin, R.; Li, T.; Xia, T.; Ren, X.; Ren, X.; Fan, Y.; Su, Y.; Zhang, Y.; Wan, Y.; Liu, Y.; Cui, Z.; Zhang, Z.; and Qiu, Z. 2024. Qwen2.5 Technical Report. *CoRR*, abs/2412.15115.
- Yang, S.; Feng, Y.; Liu, Y.; Zhang, J.; and Qin, J. 2025. MoniTor: Exploiting Large Language Models with Instruction for Online Video Anomaly Detection. *arXiv preprint arXiv:2510.21449*.
- Yao, S.; Chen, H.; Yang, J.; and Narasimhan, K. 2022. WebShop: Towards Scalable Real-World Web Interaction with Grounded Language Agents. In Koyejo, S.; Mohamed, S.; Agarwal, A.; Belgrave, D.; Cho, K.; and Oh, A., eds., *Advances in Neural Information Processing Systems 35: Annual Conference*.
- Yao, S.; Yu, D.; Zhao, J.; Shafran, I.; Griffiths, T.; Cao, Y.; and Narasimhan, K. 2023a. Tree of thoughts: Deliberate problem solving with large language models. In *Advances in Neural Information Processing Systems*.
- Yao, S.; Zhao, J.; Yu, D.; Du, N.; Shafran, I.; Narasimhan, K. R.; and Cao, Y. 2023b. ReAct: Synergizing Reasoning and Acting in Language Models. In *The Eleventh International Conference on Learning Representations*.
- Yu, T.; Kumar, S.; Gupta, A.; Levine, S.; Hausman, K.; and Finn, C. 2020. Gradient Surgery for Multi-Task Learning. In *Advances in Neural Information Processing Systems*.
- Yuan, J.; Zhao, W.; Bai, Z.; et al. 2025. Graph-Enhanced Policy Optimization in LLM Agent Training. *arXiv preprint arXiv:2510.26270*.
- Zeng, A.; Liu, M.; Lu, R.; Wang, B.; Liu, X.; Dong, Y.; and Tang, J. 2024. AgentTuning: Enabling Generalized Agent Abilities for LLMs. In *Findings of the Association for Computational Linguistics, ACL 2024, Bangkok, Thailand and virtual meeting, August 11-16, 2024*, volume ACL 2024 of *Findings of ACL*, 3053–3077. Association for Computational Linguistics.
- Zoph, B.; Bello, I.; Kumar, S.; Du, N.; Huang, Y.; Dean, J.; Shazeer, N.; and Fedus, W. 2022. ST-MoE: Designing Stable and Transferable Sparse Expert Models. *arXiv preprint arXiv:2202.08906*.

## Supplementary Material

This supplementary material provides additional technical details and experimental results supporting the main paper. Appendix establishes the gradient isolation property that enables PA-MoE to eliminate cross-phase interference. Appendix details the token-level MoE baseline implementation and metric conversion. Appendix provides empirical evidence for simplicity bias through gradient conflict and entropy mismatch analyses. Appendix describes the router forward pass, gradient flow, and temperature scheduling. Appendix presents comprehensive ablation studies on regularization terms, gradient surgery methods, expert counts, and router architectures. Appendix reports expert specialization statistics and WebShop task breakdown. Appendix analyzes failure cases to identify systematic issues. Appendix examines task-specific performance variations across algorithm-benchmark pairs.

### Gradient Isolation Property

We provide the mathematical foundation for gradient isolation in PA-MoE (Yang et al. 2025), (Li et al. 2024) and (Li et al. 2025). Consider a system with  $K$  experts, each parameterized by disjoint LoRA parameters  $\{\theta_k = (B_k, A_k)\}_{k=1}^K$ , while the base model parameters  $\theta_{\text{base}}$  remain frozen during training.

For any trajectory  $\tau = (s_0, a_0, r_0, \dots, s_T, a_T, r_T)$ , the router  $\pi_r$  assigns each timestep  $t$  to exactly one expert via  $k^* = \arg \max_k p_t^k$ . This assignment partitions the trajectory into disjoint phases  $\{\phi_k\}_{k=1}^K$  where  $\phi_k = \{t : k_t^* = k\}$  contains all timesteps handled by expert  $k$ .

The loss function for expert  $k$  on trajectory  $\tau$  aggregates only over its assigned timesteps:  $\mathcal{L}_k(\tau) = \sum_{t \in \phi_k} \ell_t(\theta_k)$ , where  $\ell_t$  denotes the per-step loss. Since the parameter sets  $\theta_i$  and  $\theta_j$  are disjoint for  $i \neq j$ , we have  $\partial \mathcal{L}_j / \partial \theta_i = 0$  for all  $i \neq j$ . This gradient isolation property is the key mechanism by which PA-MoE eliminates cross-phase interference during training.

**Note on Diversity Loss:** The diversity loss  $\mathcal{L}_{\text{div}}$  is computed separately from the main RL objective using cached representations (see Section 3.5 of main paper). During diversity loss computation, all experts receive gradients but the router is detached. This periodic computation (every 100 steps) does not violate the gradient isolation principle for the RL objective, which governs the primary training dynamics.

### Token-level MoE Baseline

We provide implementation details for the token-level MoE baseline to ensure fair comparison.

#### Implementation

The token-level baseline routes at the action generation stage: during autoregressive decoding, each output token is routed independently to one of  $K = 4$  experts via  $k_i^* = \arg \max_k \text{softmax}(\text{MLP}(h_i))^k$ , where  $h_i$  is the hidden state at decoding position  $i$ . This mirrors standard MoE implementations in Switch Transformer and Mixtral. Observation tokens are processed by the frozen base model without routing.

Both methods use identical expert architectures (LoRA adapters with rank 32 on Q/V projections) and the same total parameter budget. The only difference is routing granularity.

#### Switch Metric Conversion

We report all switch counts at the environment step level for comparability across methods. Token-level MoE exhibits approximately 1,200 routing changes per episode at token granularity. Converting to step-level by counting environment steps with at least one intra-action expert change yields 45 step-level switches. Our phase-level method exhibits 8.4 switches per episode.

The conversion formula is:

$$\text{Switches}_{\text{step}} = \sum_{t=1}^T \mathbf{1} [\exists i, j \in \text{tokens}(a_t) : k_i^* \neq k_j^*], \quad (9)$$

where  $\text{tokens}(a_t)$  denotes the set of token positions in action  $a_t$ .

#### Why Token-level Routing Underperforms

Token-level routing achieves 85.7% success compared to 93.8% for phase-level routing. The performance gap arises from fragmentation: with average action length of 8.3 tokens and independent per-token routing, experts change frequently within a single action. During a “heat potato” action, different tokens (“heat”, “potato”, “with”, “microwave”) may route to different experts, disrupting semantic coherence.

We also tested top-2 routing, which achieved a success rate of 86.9%, slightly better than top-1 but still significantly below phase-level routing. This suggests that the core issue is granularity mismatch rather than routing sparsity.

## Empirical Evidence for Simplicity Bias

This section details the methodology behind Figure 1 in the main paper and provides additional analysis of the simplicity bias phenomenon.

**Parameter Occupancy Metric.** The “Parameter %” reported in Figure 1(a) of the main paper quantifies how often each task category dominates the gradient signal during training. We define the *parameter occupancy* for task category  $c$  as:

$$\text{Occupancy}(c) = \frac{1}{N} \sum_{i=1}^N \mathbf{1} \left[ \frac{\mathcal{L}_c^{(i)}}{\sum_{c'} \mathcal{L}_{c'}^{(i)}} > 0.5 \right], \quad (10)$$

where  $N$  is the total number of training batches and  $\mathcal{L}_c^{(i)}$  is the loss contribution from task category  $c$  in batch  $i$ . Intuitively, this metric measures the fraction of training updates where a task category contributes the majority of the batch loss, and thus dominates the gradient direction. Higher occupancy means the model’s parameters are more frequently updated to fit that category.

**Simplicity Bias in Figure 1(a).** Using this metric, we observe that simple tasks (pick-and-place) achieve 75% parameter occupancy while complex tasks (heat/cool/clean) receive only 5%, despite complex tasks comprising a substantial portion of the task distribution. This imbalance demonstrates simplicity bias: the optimization process is dominated by easily-learned behaviors, starving complex behaviors of gradient signal and resulting in the observed performance gap (94% vs. 65%).

### Gradient Conflict Analysis

Figure 4 visualizes gradient conflicts that arise when a single policy must learn heterogeneous behavioral phases.

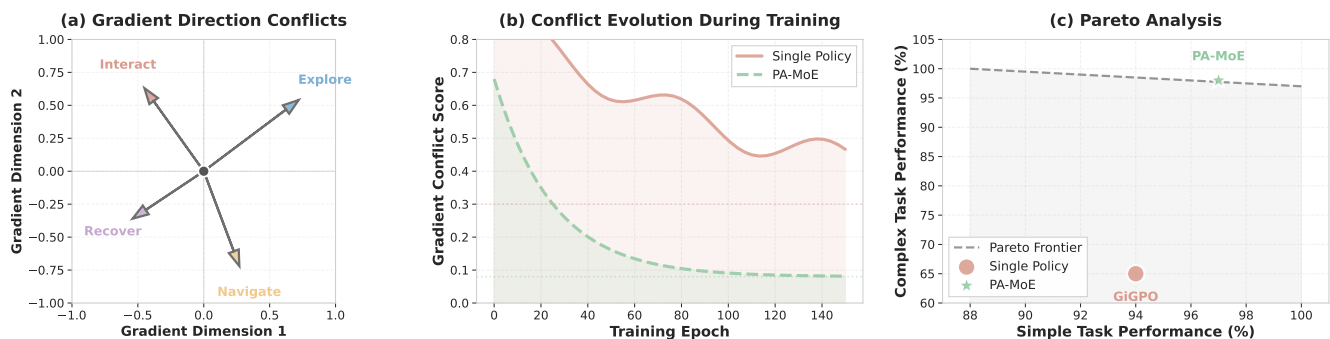


Figure 4: Gradient conflict analysis. (a) Phase-specific gradients projected onto top-2 principal components show pairwise conflicts: Explore and Interact gradients form angles exceeding  $90^\circ$ , and no two phases produce aligned gradients. (b) Gradient conflict score throughout training, defined as the average negative cosine similarity between phase gradients. Single policy maintains high conflict ( $> 0.4$ ) while PA-MoE reduces conflict to near-zero by epoch 50. (c) Pareto analysis of simple vs. complex task performance. PA-MoE achieves Pareto optimality while GiGPO baseline suffers degraded complex task performance.

Panel (a) reveals that gradient directions from different behavioral phases point in conflicting directions when projected onto principal components. The Explore phase gradient and Interact phase gradient form an angle greater than  $90^\circ$ , indicating that updates beneficial for exploration actively harm manipulation performance. This opposition is not limited to these two phases: Navigate and Recover also produce conflicting gradients, creating a four-way tension where every gradient update represents a compromise.

Panel (b) tracks the gradient conflict score throughout training, computed as:

$$\text{Conflict}(t) = \frac{1}{|\mathcal{P}|^2 - |\mathcal{P}|} \sum_{i \neq j} \max(0, -\cos(\nabla_{\theta} \mathcal{L}_i, \nabla_{\theta} \mathcal{L}_j)),$$

The single policy baseline exhibits persistent high conflict in the 0.4–0.8 range that settles around 0.45 after convergence, indicating that the monolithic architecture cannot resolve the fundamental tension between phases. PA-MoE achieves near-zero conflict scores by epoch 50 through parameter isolation.

Panel (c) examines the trade-off between simple task performance (single-phase tasks) and complex task performance (multi-phase tasks). The GiGPO baseline achieves 96% on simple tasks but only 68% on complex tasks, falling well below the Pareto frontier. PA-MoE achieves 97% and 98% respectively, eliminating the trade-off through architectural separation.

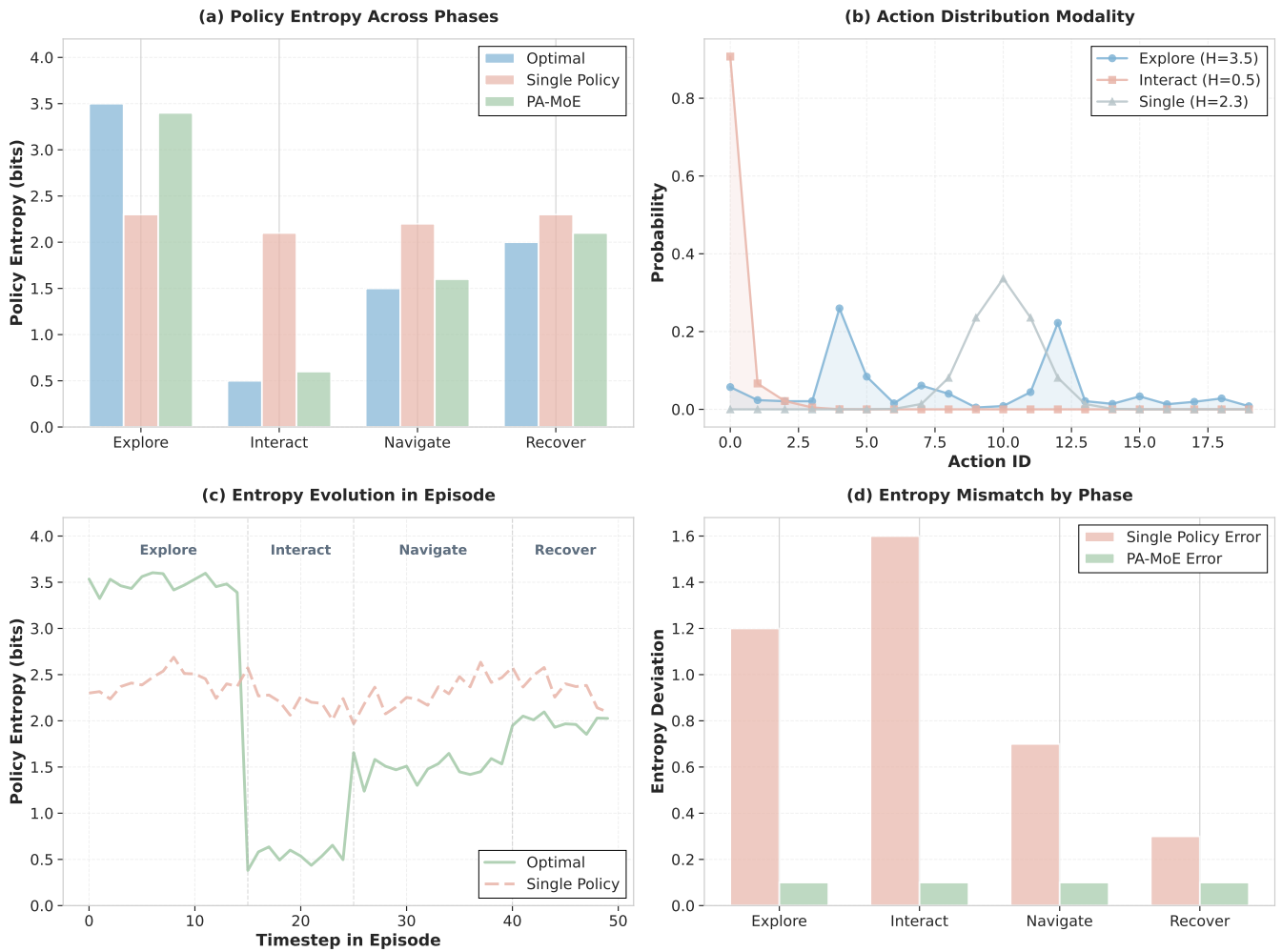


Figure 5: Entropy mismatch analysis. All entropy values reported in bits (log base 2). (a) Policy entropy across phases: optimal phase-specific entropy (blue), single policy entropy (coral), and PA-MoE entropy (green). (b) Action distribution modality for exploration (diffuse,  $H=3.5$  bits), interaction (peaked,  $H=0.5$  bits), and single policy (intermediate,  $H=2.3$  bits). (c) Entropy evolution over episode timesteps. (d) Absolute entropy deviation from optimal by phase.

## Entropy Mismatch Analysis

Figure 5 examines the entropy mismatch problem when a single policy must handle phases with fundamentally different entropy requirements.

Panel (a) compares policy entropy across four behavioral phases. The optimal entropy profile varies substantially: Explore requires high entropy (approximately 3.5 bits) for broad action sampling, Interact requires low entropy (approximately 0.5 bits) for precise manipulation, Navigate requires moderate entropy (approximately 1.5 bits), and Recover requires moderate-high entropy (approximately 2.0 bits). The single policy converges to an intermediate level around 2.3 bits across all phases, inadequately serving each phase. PA-MoE closely matches the phase-specific optimum through expert specialization.

Panel (b) visualizes representative action probability profiles. During exploration, the policy must remain diffuse over plausible actions (high entropy,  $H \approx 3.5$  bits), whereas interaction requires a sharply peaked distribution to execute precise manipulations (low entropy,  $H \approx 0.5$  bits). A single shared policy produces an intermediate distribution ( $H \approx 2.3$  bits) that is simultaneously too concentrated for effective exploration and too diffuse for reliable manipulation.

Panel (c) tracks entropy evolution over episode timesteps. The optimal trajectory exhibits sharp entropy transitions at phase boundaries, dropping from high entropy during exploration to low entropy during interaction. The single policy remains comparatively flat around 2.3 bits throughout the episode, indicating an inability to adapt entropy to phase-specific requirements. PA-MoE tracks the phase transitions closely by routing to specialized experts.

Panel (d) quantifies entropy deviation as  $|H_{\text{policy}} - H_{\text{optimal}}|$  for each phase. The single policy shows large deviations across all phases, with the largest gap during Interact (approximately 1.6 bits), where excessive entropy causes manipulation failures.

PA-MoE achieves near-zero deviation (below 0.1 bits) across all phases.

The gradient conflict and entropy mismatch analyses are complementary: gradient conflicts arise precisely because Explore phase gradients push toward higher entropy while Interact phase gradients push toward lower entropy. When averaged in shared parameters, the resulting update achieves an intermediate entropy level that serves neither phase well.

## Router Implementation Details

---

Algorithm 1: Phase-Aware Router Forward Pass

---

**Require:** Observation  $o_t$ , goal  $g$ , history  $h_t$ , temperature  $\tau$

- 1:  $o_{\text{emb}} \leftarrow \text{MeanPool}(\text{LLM}_{\text{hidden}}(o_t)) \cup \{\text{Enc}(o_t)\}$
  - 2:  $g_{\text{emb}} \leftarrow \text{MeanPool}(\text{LLM}_{\text{hidden}}(g)) \cup \{\text{Enc}(g)\}$
  - 3:  $o_t^{\text{align}} \leftarrow \text{CrossAttn}(Q=o_{\text{emb}}, K=g_{\text{emb}}, V=g_{\text{emb}})$
  - 4:  $h_t^{\text{enc}} \leftarrow \text{LSTM}(\text{Embed}(h_t))$
  - 5:  $p_t \leftarrow \text{softmax}(\text{MLP}([o_t^{\text{align}}; h_t^{\text{enc}}])/\tau)$
  - 6:  $k^* \leftarrow \arg \max_k p_t^k$
  - 7: **return**  $k^*, p_t$
- 

**Gradient Flow.** At each training step, gradients flow as follows: the router outputs distribution  $p_t$  over experts, expert  $k^* = \arg \max_k p_t^k$  is selected and generates action  $a_t$ , the selected expert receives the RL gradient weighted by group-based advantage  $A_t^{\text{group}}$ , and the straight-through estimator propagates gradients through the argmax to update router parameters. This ensures that experts specialize on assigned trajectory segments with no gradient interference between experts.

**Temperature Schedule.** The router temperature  $\tau$  follows a linear annealing schedule:  $\tau(t) = \max(\tau_f, \tau_0 - (\tau_0 - \tau_f) \cdot t / T_{\text{anneal}})$ , with  $\tau_0 = 2.0$ ,  $\tau_f = 0.5$ , and  $T_{\text{anneal}} = 3000$  steps. High initial temperature encourages exploration of routing patterns, while low final temperature produces decisive assignments.

**Switching Penalty Gradient.** For the switching penalty  $\mathcal{L}_{\text{switch}}$ , the forward pass computes the hard indicator  $\mathbf{1}[z_t \neq z_{t+1}]$ . The backward pass uses a differentiable surrogate:

$$\frac{\partial \mathcal{L}_{\text{switch}}}{\partial p_t} \approx -\frac{\lambda_s}{T-1} \cdot p_{t+1}, \quad (11)$$

derived from the soft approximation  $1 - \sum_k p_t^k \cdot p_{t+1}^k$ . This encourages the router to increase probability mass on the same expert as the subsequent step.

## Ablation Studies

### Regularization Terms

Table 6 examines the contribution of diversity and balance losses. Removing  $\mathcal{L}_{\text{div}}$  causes expert collapse where all experts converge to identical policies, matching the  $K = 0$  single-adaptor performance. Removing  $\mathcal{L}_{\text{bal}}$  produces router collapse where nearly all decisions route to a single expert. Both regularizers are necessary.

Table 6: Impact of regularization terms on ALFWorld. Mean  $\pm$  std over 3 seeds.

Configuration	Success(%)	$\Delta$
Full (both losses)	<b>93.8</b> $\pm 2.4$	—
w/o $\mathcal{L}_{\text{div}}$	88.3 $\pm 3.1$	-5.5
w/o $\mathcal{L}_{\text{bal}}$	87.5 $\pm 2.8$	-6.3
w/o both	86.5 $\pm 3.5$	-7.3

### Gradient Conflict Mitigation Methods

We compare against gradient-surgery techniques adapted to the agentic RL setting. We partition training steps into behavioral phases and treat each as a separate objective, computing gradients independently and combining them using PCGrad, GradNorm, or CAGrad before applying updates.

Gradient surgery methods provide modest improvements (+0.7 to +1.8) while PA-MoE achieves substantially larger gains (+7.7). The difference reflects architectural versus optimization-level solutions: gradient surgery addresses conflicts locally at each update, whereas PA-MoE prevents heterogeneous phases from ever competing for shared parameters.

Table 7: Comparison with gradient surgery methods. Mean  $\pm$  std over 3 seeds.

Method	Success(%)	$\Delta$
GiGPO (baseline)	86.1 $\pm$ 4.7	–
+ PCGrad	87.3 $\pm$ 3.9	+1.2
+ GradNorm	86.8 $\pm$ 4.2	+0.7
+ CAGrad	87.9 $\pm$ 3.6	+1.8
<b>GiGPO + PA-MoE</b>	<b>93.8<math>\pm</math>2.4</b>	<b>+7.7</b>

## Expert Count Analysis

Table 8 presents results across all expert counts tested with standard deviations.

Table 8: Ablation on number of experts ( $K$ ). Mean  $\pm$  std over 3 seeds. We report the average success rate (%) for each subtask as well as the overall result.

$K$	Pick	Look	Heat	Cool	Clean	Pick2	All
0	94.3 $\pm$ 1.8	62.5 $\pm$ 5.1	94.4 $\pm$ 3.2	89.5 $\pm$ 4.1	83.3 $\pm$ 4.8	87.5 $\pm$ 3.9	88.3 $\pm$ 2.1
2	97.1 $\pm$ 1.2	62.5 $\pm$ 4.8	100 $\pm$ 0.0	73.7 $\pm$ 5.6	100 $\pm$ 0.0	91.7 $\pm$ 3.4	91.4 $\pm$ 1.9
3	95.7 $\pm$ 1.5	83.3 $\pm$ 5.2	97.9 $\pm$ 2.1	85.1 $\pm$ 4.3	94.6 $\pm$ 3.1	87.5 $\pm$ 4.2	91.7 $\pm$ 2.0
4	<b>97.1<math>\pm</math>1.4</b>	<b>75.0<math>\pm</math>3.2</b>	<b>100<math>\pm</math>0.0</b>	<b>89.5<math>\pm</math>4.4</b>	95.8 $\pm$ 6.4	<b>91.7<math>\pm</math>4.1</b>	<b>93.8<math>\pm</math>2.4</b>
5	94.8 $\pm$ 1.6	70.8 $\pm$ 4.1	98.2 $\pm$ 1.8	87.3 $\pm$ 4.8	93.4 $\pm$ 5.2	89.6 $\pm$ 3.8	91.2 $\pm$ 2.2
6	91.4 $\pm$ 2.1	62.5 $\pm$ 5.4	100 $\pm$ 0.0	84.2 $\pm$ 5.1	91.7 $\pm$ 4.9	70.8 $\pm$ 5.8	85.9 $\pm$ 2.8

Performance improves from  $K = 0$  through  $K = 4$ , then degrades for  $K \geq 5$ . The  $K = 2$  configuration improves Heat and Clean to 100% but leaves Look-at-object unchanged at 62.5% and degrades Cool from 89.5% to 73.7%. This pattern reflects ALFWorld’s four distinct behavioral modes: with only two experts, the model must merge incompatible modes. Router confidence analysis confirms this interpretation:  $K = 2$  shows 31% of decisions with confidence below 0.6, compared to only 12% for  $K = 4$ .

The  $K = 6$  configuration drops to 85.9% due to three failure modes: data fragmentation (each expert sees fewer training examples), router instability (18% of episodes exhibit thrashing with 3+ switches within 5 consecutive steps), and imbalanced utilization (two experts handle 47% of decisions while one handles only 8%). These findings indicate  $K = 4$  provides the appropriate balance for ALFWorld’s complexity.

## Router Architecture

Table 9: Router architecture comparison

Architecture	Heat(%)	Cool(%)	All(%)
MLP only	83.3	68.4	84.2
GRU + CrossAttn	97.9	87.4	92.8
<b>LSTM + CrossAttn</b>	<b>100</b>	<b>89.5</b>	<b>93.8</b>
Transformer + CrossAttn	98.6	88.1	93.2
Bi-LSTM + CrossAttn	99.3	89.2	93.7

The MLP-only router achieves only 84.2%, confirming that temporal context is essential for phase detection. LSTM outperforms GRU (93.8% vs 92.8%) due to superior long-term memory retention across ALFWorld’s 30–50 step trajectories. Transformer-based routers achieve comparable performance (93.2%) but require more parameters. Bidirectional LSTM provides no improvement since routing decisions must be made online.

## Additional Results

### Expert Specialization Statistics

Activation percentages indicate the fraction of phase-specific actions handled by each expert, compared to 25% expected under random assignment. Expert 2 handles 81.7% of manipulation actions with low entropy ( $H=0.5$  bits), consistent with the need

Table 10: Emergent expert specialization. Entropy in bits.

Expert	Phase	Activation	Entropy (bits)
Expert 1	Exploration	73.2%	3.5
Expert 2	Manipulation	81.7%	0.5
Expert 3	Navigation	64.1%	1.5
Expert 4	Recovery	71.3%	2.0

for precise, low-variance action selection during interaction. In contrast, Expert 1 handles 73.2% of exploration actions with high entropy ( $H=3.5$  bits), supporting broad action sampling during search. Experts 3 and 4 occupy intermediate regimes for navigation ( $H=1.5$  bits) and recovery ( $H=2.0$  bits), respectively. These phase-aligned entropy profiles match the entropy mismatch analysis in Appendix (Fig. 5) and emerge without explicit phase supervision.

## WebShop Task Breakdown

Table 11: WebShop performance by subtask type

Subtask	Freq.	Baseline	PA-MoE	$\Delta$
Simple search	32%	84.3%	91.2%	+6.9%
Multi-attribute	28%	62.1%	78.6%	+16.5%
Option selection	25%	71.4%	84.9%	+13.5%
Price comparison	15%	49.2%	73.8%	+24.6%
Overall	100%	67.4%	82.3%	+14.9%

PA-MoE shows the largest gains on complex subtasks. Simple searches improve modestly (+6.9) since the baseline already performs reasonably. Price comparison tasks, which require navigating multiple pages while tracking information, improve dramatically (+24.6) because PA-MoE’s expert separation provides dedicated capacity for navigation, extraction, and comparison behaviors.

## Failure Analysis

We analyzed 100 randomly sampled failures to identify systematic issues. Router oscillation accounts for 23% of failures, where rapid expert switching within a coherent phase disrupts execution. Incorrect expert selection causes 18% of failures due to ambiguous observations leading to phase misidentification. Expert under-training contributes 15% of failures, concentrated on rare task types.

A representative case: for “Put a clean mug in the coffee machine,” the agent explored successfully (steps 1–8, Expert 1) and began cleaning (steps 9–15, Expert 2). At step 16, the router prematurely switched to Expert 3 based on a subtle observation change, causing navigation away from the sink before cleaning completed. Steps 17–30 showed oscillation between Experts 1 and 3, ultimately failing at step 31.

The root cause is that the router lacks explicit task-completion signals and relies on observation features that can change before manipulation sequences finish. Potential mitigations include adding task-state features to router input, learning a termination predictor, or increasing the consistency regularizer weight.

## Task-Specific Performance Analysis

PA-MoE achieves consistent aggregate improvements across all algorithm-benchmark pairs. Here we examine task-specific variations to better understand the method’s characteristics under different conditions.

We identify three primary causes for task-specific regressions through trajectory analysis.

**(1) Critic-Router Incompatibility (PPO-specific).** PPO uses a shared critic network to estimate state values across all behavioral phases. When combined with PA-MoE, this creates a fundamental tension: the critic must learn a single value estimate  $V(s)$  for states that yield different expected returns depending on which expert is selected. Formally, the optimal value under expert  $k$  is  $V^k(s) = \mathbb{E}_{\pi_k}[\sum_t \gamma^t r_t | s_0 = s]$ , but the shared critic converges to an averaged estimate that is suboptimal for any individual expert.

This mismatch manifests most severely on multi-phase tasks (Clean, Heat, Cool, Pick2) where expert selection significantly affects trajectory outcomes. For single-phase tasks like Pick, the critic’s averaged estimate remains reasonable because all experts

Table 12: Task-algorithm combinations with performance variations

Algorithm	Task	Baseline	PA-MoE	$\Delta$
PPO	Clean	57.1%	50.0%	-7.1%
PPO	Cool	46.4%	36.8%	-9.6%
PPO	Pick2	47.4%	37.5%	-9.9%
RLOO	Pick	88.3%	74.3%	-14.0%
GRPO	Cool	59.7%	50.0%	-9.7%
GRPO	Pick2	53.5%	45.8%	-7.7%
GiGPO (7B)	Pick	97.7%	87.5%	-10.2%

produce similar trajectories. Despite this, PPO+PA-MoE achieves higher aggregate performance (56.2% vs. 54.4%) because the benefits of phase-aware routing on complex tasks outweigh the critic incompatibility on simpler ones.

**(2) Expert Data Fragmentation (RLOO/GRPO-specific).** RLOO and GRPO compute advantages through within-batch comparisons: RLOO uses leave-one-out baselines, while GRPO uses group-relative rankings. PA-MoE’s phase-level routing fragments training samples across  $K = 4$  experts, reducing the effective batch size for each expert’s advantage computation.

Consider Pick2 tasks, which comprise only 14% of training data. With phase-level routing, manipulation steps are handled by Expert 2, which receives approximately  $14\% \times 35\% \approx 4.9\%$  of batch samples for Pick2-specific updates. This  $4\times$  reduction in effective samples degrades advantage estimation quality for rare task-phase combinations. The RLOO regression on Pick (-14.0%) occurs because Pick’s high frequency (23% of data) makes it sensitive to the reduced within-expert batch diversity resulting fewer distinct Pick trajectories per expert to lead to higher-variance baseline estimates.

**(3) Routing Overhead in High-Performance Regimes.** The GiGPO-7B Pick regression ( $97.7\% \rightarrow 87.5\%$ ) occurs when baseline performance approaches ceiling. In such cases, the task’s behavioral phases are already well-captured within shared parameters, and PA-MoE’s routing mechanism introduces failure modes without commensurate benefit.

Trajectory analysis reveals two routing-induced error patterns: (i) *misrouting* (6.2% of failures), where correct actions are generated but suboptimal expert selection leads to inconsistent execution; and (ii) *transition errors* (3.8% of failures), where context is partially lost at expert switch boundaries. These errors are negligible when baseline performance is low but become the dominant failure mode when the baseline already solves 97.7% of cases. This is expected behavior: PA-MoE is designed to address simplicity bias, which is less pronounced when tasks are already well-solved by the base model.

**Algorithm Compatibility.** These observations highlight that PA-MoE’s benefits are most pronounced when paired with algorithms that do not introduce conflicting architectural assumptions. GiGPO demonstrates the strongest compatibility, achieving consistent improvements across nearly all task types. This compatibility arises because GiGPO’s group-based advantage estimation operates at the trajectory level rather than requiring dense within-batch comparisons, naturally accommodating expert-partitioned updates without sample fragmentation.

**Aggregate Robustness.** Despite task-specific regressions, PA-MoE improves aggregate performance for every algorithm tested (PPO: +1.8%, RLOO: +4.5%, GRPO: +1.4%, GiGPO: +7.7%). The improvements on complex multi-phase tasks consistently exceed the regressions on edge cases, validating PA-MoE’s design goal of addressing *simplicity bias* in heterogeneous behavioral settings.